



Measurement of Projections Between Dentate Nucleus and Contralateral Frontal Cortex in Human Brain Via Diffusion Tensor Tractography

Qing Ji¹ · Angela Edwards¹ · John O. Glass¹ · Tara M. Brinkman^{2,3} · Zoltan Patay¹ · Wilburn E. Reddick¹

Published online: 6 May 2019

© Springer Science+Business Media, LLC, part of Springer Nature 2019

Abstract

We propose a probabilistic fiber-tracking scheme to reconstruct the fiber tracts between the dentate nucleus (DN) in the cerebellum and the entire contralateral cerebral frontal cortex in the human brain. We assessed diffusion tensor imaging (DTI) data from 39 healthy controls. The connection fibers between the DN and contralateral frontal cortex of all subjects were successfully reconstructed and studied. We demonstrated that multi-fiber probabilistic models must be used to resolve the challenge of crossing fibers. We also demonstrated that the entire pathway can be reconstructed without using any synaptic regions of interest along the path and that the reconstructed tracts connected the ipsilateral superior cerebellar peduncle, contralateral red nucleus, and ventral lateral and ventral anterior nuclei of thalamus in the path traveling to the contralateral frontal cortex. The fibers in the pathway projected into all areas of the contralateral frontal cortex but were predominantly located in the primary motor and premotor areas. A large portion of fibers terminated in the prefrontal cortex, which included dorsolateral prefrontal areas, anterior prefrontal areas, and the Broca language area. Our findings provide robust, reproducible, and direct DTI-based evidence that the DN through the efferent cerebellar pathway has considerable contribution to high-level executive functions of the human brain.

Keywords Cerebellum · Clustering · Dentate nucleus · Diffusion tractography · Frontal cortex

Introduction

The pathway between the deep cerebellar nucleus and the contralateral cerebral cortex constitutes the efferent part of the cerebral-cerebellar connection loop. Ascending from the dentate nucleus (DN) with possible contributions from the adjacent emboliform, globous, and fastigial nuclei, the efferent cerebellar pathway includes the following structures: the ipsilateral superior cerebellar peduncle (SCP), decussation of

the superior cerebellar peduncles in the pontomesencephalic tegmentum, contralateral red nucleus (RN), the thalamus, and contralateral cerebral cortex. Because all of the fibers in this pathway pass through the contralateral thalamus, it is referred to as the cerebello-thalamo-cerebral (CTC) or dentato-rubro-thalamo-cortical pathway. The connection between the DN and the contralateral frontal cortex forms the dominant part of the CTC pathway, although other connections exist, such as the connections with the contralateral parietal cortex and temporal cortex. For simplification purposes, we refer to the connection pathway between the DN and the contralateral frontal cortex as the CTC pathway here. The CTC pathway can be divided into two major portions. The first portion, the dentatorubrothalamic tract (DRTT), extends from the DN to the contralateral thalamus and the proximal, dentato-rubral segment of that tract also constitutes the first ascending leg of the Guillain–Mollaret triangle [1]. The second portion comprises the fiber bundles from the thalamus to the frontal cortex (i.e., thalamo-cortical projections).

The CTC pathway, which transmits cerebellar input to the supratentorial brain, is indispensable for the coordination of

✉ Qing Ji
qing.ji@stjude.org

¹ Department of Diagnostic Imaging, St. Jude Children's Research Hospital, 262 Danny Thomas Place, MS 220, Memphis, TN 38105-3678, USA

² Department of Psychology, St. Jude Children's Research Hospital, Memphis, TN, USA

³ Department of Epidemiology and Cancer Control, St. Jude Children's Research Hospital, Memphis, TN, USA

movement and plays many important roles in cognitive functions, such as planning, verbal communication, working memory, abstract thinking, and behavior [2]. Disruption of the CTC pathway can result in abnormal movement, ataxia, tremor, and cerebellar cognitive affective syndrome (CCAS) [3]. In patients with midline, intraventricular posterior fossa tumors such as medulloblastoma, the CTC pathway, particularly that in the DRTT, can be damaged during surgery. This damage, especially if bilateral, may result in postoperative cerebellar mutism syndrome, which is considered the extreme form of CCAS [4–8]. The CTC pathway, especially the DRTT portion in the cerebellum, is also an important target for deep-brain stimulation, which is a well-established option for treatment of movement disorders such as Parkinson disease [9–11].

Although the CTC pathway is one of the largest fiber tract systems in the central nervous system, the cortical areas affected by the CTC pathway are not well defined. In clinical practice, accurate identification of the CTC pathway, especially the DRTT (in both healthy and diseased tissue), may be useful for surgical planning in the posterior fossa. However, it is very difficult to directly identify the CTC pathway located outside of the SCP with conventional computed tomography and magnetic resonance (MR) images [12, 13].

Diffusion tensor imaging (DTI) tractography uses the anisotropic property of water diffusion in white matter to reconstruct three-dimensional (3D) brain neural fiber tracts in vivo [14]. The first part (i.e., the DRTT) [4, 11, 15] and second part (i.e., thalamo-cortical projections) [16, 17] of the CTC pathway have been extensively studied with DTI tractography. However, very few studies have examined the entire CTC pathway [18–21], and those studies did not provide detailed information about which cortical areas are connected by the CTC pathway. The major challenge for reconstruction of the CTC pathway is that it traverses several regions where fiber tracts merge or cross. Therefore, tracking the CTC pathway relies heavily on the ability to resolve the “crossing fiber challenge” in the tractography algorithm. To overcome this challenge, some studies suggest using advanced technologies, such as constrained spherical deconvolution [22], high angular resolution diffusion imaging [19, 23], or diffusion spectrum imaging [24] to reconstruct the CTC pathway or DRTT.

Here, we propose a relatively simple approach. We demonstrate that the entire CTC pathway can be reconstructed by combining probabilistic fiber tracking and streamline clustering techniques by using DTI data acquired in a clinical environment. Although the CTC pathway is a long and complex multi-synaptic tract, in our approach, the only synaptic regions of interest (ROIs) we used were seed (DN) and target (entire contralateral frontal cortex) ROIs. We demonstrate that the reconstructed CTC pathway not only connects the ipsilateral SCP, contralateral RN, and thalamus but also describes in detail the contralateral frontal cortical areas that are connected.

Materials and Methods

Subjects

MR imaging was acquired from 39 healthy volunteers (mean age, 23.84 ± 4.39 years). Of these, 36 were right handed, and 3 were left handed. None of the subjects had a history of neurologic illness. Handedness information was evaluated by using the Edinburgh Handedness Inventory [25] and then converted into a binary reading. The study was approved by the Institutional Review Board and was conducted in accordance with guidelines from the National Cancer Institute and Office for Human Research Protection. Informed consent was obtained from each subject or parent/guardian, as appropriate.

MR Image Acquisitions

MR examinations consisted of a 3D structure T_1 -weighted image set and DTI. The T_1 -weighted images were acquired by using the sagittal MPRAGE sequence (TR/TE 1980 ms/2.26 ms, 1.0-mm pixel space, 256×256 matrix, 160 slices, and 1.0-mm slice thickness). The DTIs were acquired with a multi-band single-shot echo-planar imaging sequence (TR/TE 4000 ms/78.6 ms, 64 gradient directions, b value 1500, single b_0 image, 1.8-mm pixel space, 128×128 matrix, 108 slices, and 1.8-mm slice thickness; 2 acquisitions).

Image Preprocessing

The T_1 -weighted structure image was resampled into 256 axial slices and then processed with Freesurfer (<http://surfer.nmr.mgh.harvard.edu>) for cortical parcellation [26, 27]. Sixty-eight cortical structures (34 on each hemisphere) and 14 (7 on each hemisphere) subcortical structures (including left and right thalamus) were obtained after processing. The DTI were preprocessed with the Functional Magnetic Resonance Imaging of the Brain (FMRIB) Diffusion Toolbox [28] (<http://www.fmrib.ox.ac.uk/fsl>), which included image transfer, format conversion, eddy current, and motion artifact correction. DTI parameters were determined on a voxel basis by using DTIFIT. Alignment of the DTI and T_1 -weighted images was accomplished by using a 12-parameter affine registration.

Choice of ROIs

Two fundamental ROIs were required for tracking the CTC pathway: the DN (seed ROI) and the contralateral frontal cortex (target ROI). The left and right frontal cortex images were obtained by combing 13 cortical regions from 34 outputs of Freesurfer parcellation on each side. The left and right DNs were segmented by using a special unbiased atlas template of the human cerebellum [29]. Both the DN

and the frontal cortex were segmented on T_1 -weighted images and then transferred to the native subject DTI space (Fig. 1). For demonstration purposes, the left and right SCPs and RNs were manually segmented on the T_1 -weighted images for all subjects by an experienced researcher who followed the guidance of previously published anatomic reports [30, 31]. The left and right thalamus were included in the Freesurfer output. To analyze the frontal cortex, the Brodmann atlas was also downloaded from DSI Studio (<https://dsi-studio.labsolver.org>) and registered to each of the individual T_1 -weighted images.

Probabilistic Streamline Tractography

The FMRIB software BEDPOSTX calculates the streamline-orientation distributions by using a ball-and-stick partial-volume model. As an initial investigation, data from each subject were processed with one- to five-fiber models in BEDPOSTX to determine which model adequately resolved the crossing fibers challenge [28]. A streamline was generated in FMRIB from a seed voxel and extended along the direction that was randomly sampled from the voxel-wise orientation distribution (pre-calculated from BEDPOSTX). We used a similar streamline-generation procedure in a single- or multi-fiber-model field [28]. To this end, we created a tractography program to generate streamlines from each seed and collected all of the streamlines that reached the target. In our program, a streamline was limited to 150 mm in length and 0.5 mm in step size (maximum total of 300 segments). For each seed voxel, 1000 to 5000 streamlines were generated. Only

those streamlines that reached the defined target were collected, and these were then truncated to keep only the portion that extended from seed to target voxels. Streamlines from all of the seed voxels formed a large preliminary fiber bundle that was saved in a file format that could be read, analyzed, and displayed with TRACKVIS software (<http://trackvis.org>). Because this preliminary bundle contained all tracts connecting the seed (i.e., DN) and target (i.e., contralateral frontal cortex) voxels, it was expected to include the CTC pathway.

Streamline Clustering

A generic fiber-clustering technique based on a similarity measure was used to group the collected fibers into several similarity closed bundles. The similarity between two streamlines is defined and illustrated in Fig. 2 [32]. This similarity measure credited shape and location closeness of two streamlines and gave a penalty to the length difference. A single streamline was randomly chosen from the collected fibers and set as the centroid of a cluster. The similarities between the centroid of this cluster and other streamlines were calculated. The streamlines with similarities above an empirical threshold of 0.1 were labeled as the same cluster as the centroid. Those with similarities below the threshold remained unclustered. The process was repeated for the rest of the unclustered streamlines until all the streamlines in the bundle were clustered. The iteration terminated when several connective single-fiber groups were formed. The similarity threshold determined how many fiber bundles could be grouped.

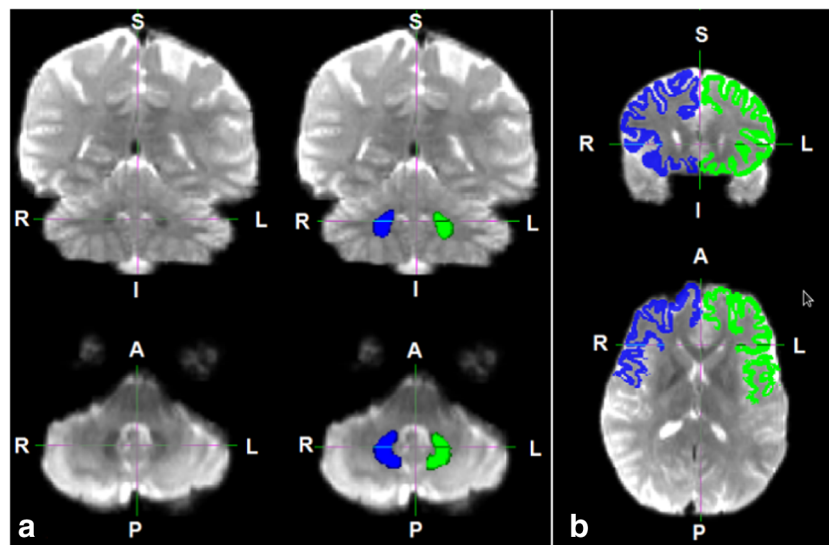
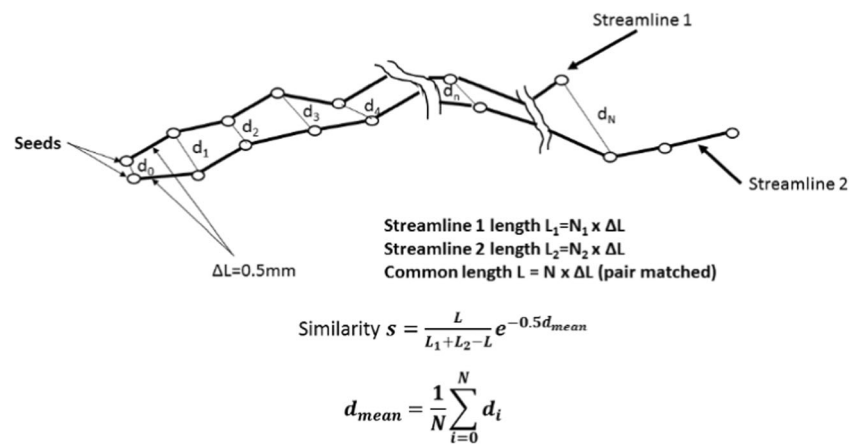


Fig. 1 Regions of interest (ROI). **a** The dentate nucleus (DN) served as the seed ROI. Left panels show coronal and axial slices of the original diffusion tensor image (DTI), with b value = 0. The left and right DN can be distinguished by the dark bean-shaped areas on the axial slice. Right

panels show the autosegmented left (green) and right (blue) DN overlaid on the DTI. **b** The entire contralateral frontal cortex (gray matter) served as the target ROI. The left (green) and right (blue) frontal cortex were also overlaid on the DTI

Fig. 2 Illustration of the similarity calculation between two streamlines. The minimum distance between any two seed points along streamline 1 and streamline 2 are calculated (d_0, d_1, \dots, d_n) and then averaged to generate the mean Euclidean distance between the two streamlines



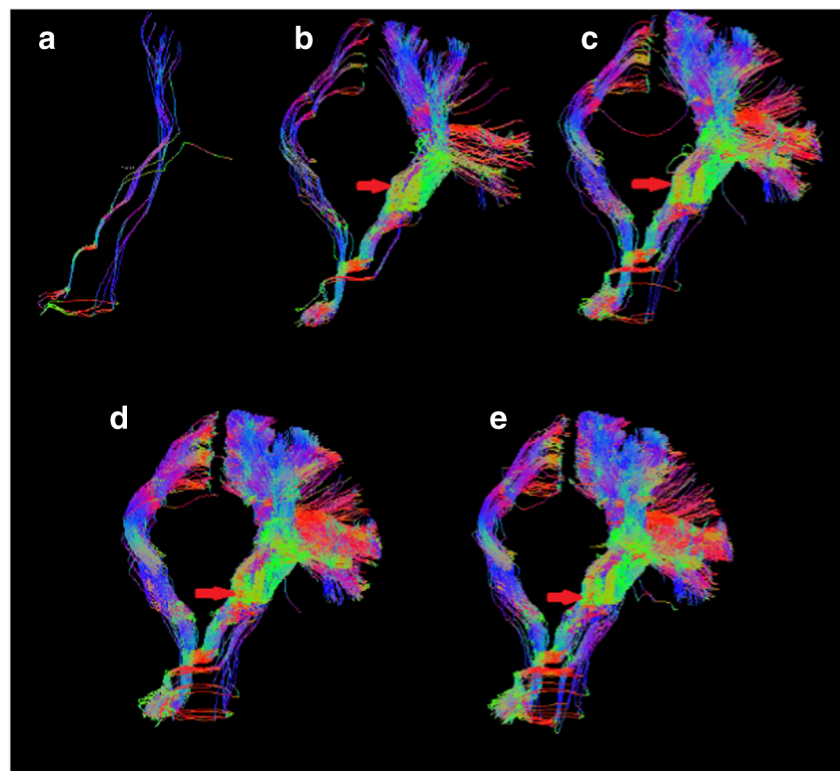
Results

Probabilistic Streamline Fiber Tracking

We first collected all possible streamlines that connected the DN and contralateral frontal cortex. The collection of these streamlines formed the preliminary bundle. The pathway from the DN to the contralateral frontal cortex was long, and only a small portion of generated streamlines reached the target to form the preliminary bundle. We tracked fibers in the fiber fields calculated by BEDPOSTX with one- to five-fiber model options. Figure 3 depicts all of the collected fibers that connected the right DN to the left frontal cortex in one to five fiber fields for a typical subject. Only a few streamlines were

collected when tracking the fibers in a single-fiber field (Fig. 3a); therefore, a one-fiber model was not suitable for tracking the CTC pathway. In the two-fiber model, the collected fibers in multiple fiber fields formed several bundles that represented the typical pathway from the DN to the contralateral frontal cortex. Among those bundles, one unique bundle crossed the midbrain (Fig. 3b–e, red arrows). On the basis of anatomic descriptions, we hypothesized that this special fiber bundle was the CTC pathway. The fibers of the CTC pathway tracked in the four- and five-fiber fields displayed more cortical connections than did those in the two- and three-fiber fields. Upon comparing the tracts obtained in the four- and five-fiber fields, we found that they contained a similar number of tracts and cortical connections. In our analyses of all of

Fig. 3 The preliminary bundles traced in multi-fiber fields. A typical right preliminary fiber bundle (right dentate to left frontal) traced from the traced from the one-, two-, three-, four-, and five-fiber fields. The fibers were direction coded



the subjects, we found that the five-fiber model was more consistent throughout all subject data; therefore, all of the results described below were calculated with the five-fiber model.

Streamline Clustering

After obtaining the left and right preliminary bundles, we separated the CTC pathway from the rest of the streamlines. We used the fiber-clustering technique described above to separate the streamlines. A typical preliminary fiber bundle is shown in Fig. 3e, which was obtained in a five-fiber field. The fibers in the preliminary bundle were bundled into several sub-bundles, which were well separated in 3D space in the cerebellum. With the tracts ascending, the fibers in each sub-bundle began to diverge. If we directly used the similarity-based clustering algorithm to group the fibers in the preliminary bundle, the entire CTC bundle could not be extracted because the fiber trajectories in each sub-bundle, especially in the CTC candidate pathway, were very different in the cortical region. To extract the entire CTC candidate pathway, we applied the clustering algorithm to only the inferior portion (starting at the DN and ascending 150 segments) of the fibers. Applying an empirical similarity value of 0.1, we effectively separated the CTC candidate pathways from the rest of the fibers (Fig. 3e). In this case, four primary sub-bundles (Fig. 4, top panel, white arrows) in the preliminary bundle were separated. We performed the actual similarity calculation on the bottom 150 segments of each fiber in the bundle (Fig. 3, top right panel). The separated four main sub-bundles are shown in the bottom panel of Fig. 4. The CTC pathway was identified as group 2. Across all of the subjects, we clustered

the left and right preliminary bundles with this strategy. The number of clusters for each preliminary bundle ranged from three to nine. We visually identified the left and right CTC pathways from the clusters because of their unique trajectories.

The Trajectory and Synaptic Connection

We extracted the left and right CTC pathways from each subject independently and then joined them together to form a full CTC tract for each subject. We successfully reconstructed the full CTC pathways of 39 healthy subjects. We observed similar CTC trajectories for all subjects. Figure 5 depicts the CTC pathways from three representative subjects. The left and right CTC pathways were symmetrical across all subjects. From the DN to the contralateral frontal cortex, the key synaptic structures along the CTC tract, including ipsilateral SCPs, contralateral RNs, and the thalamus, were connected. By overlaying the manually segmented left and right SCPs and RNs and the left and right thalamus segmented by Freesurfer, we found that all of these synaptic structures were connected by the CTC pathway. The CTC pathways originated from the DN (Fig. 6a), passed through the ipsilateral SCPs (Fig. 6b), decussated the hemisphere just above the pontomesencephalic junction (Fig. 6c), and passed through the contralateral RNs (Fig. 6d) and contralateral thalamus (Fig. 6e). The CTC pathways passed through the anterior limb of the internal capsules toward the frontal cortex (Fig. 6f). Quantitatively, for each subject, the proportion of left and right CTC fibers that completely passed through the ipsilateral SCPs were 100%. Moreover, 85 to 98% passed through contralateral RNs, and 100% passed through the contralateral thalamus.

Fig. 4 Clustering of the preliminary bundle. Top left panel, a typical right preliminary bundle. It includes four sub-bundles. Top right panel, the lower portion of the bundle in which the clustering process was actually performed. Bottom panel, the four sub-bundles were successfully separated. The right CTC pathway was defined as cluster 2

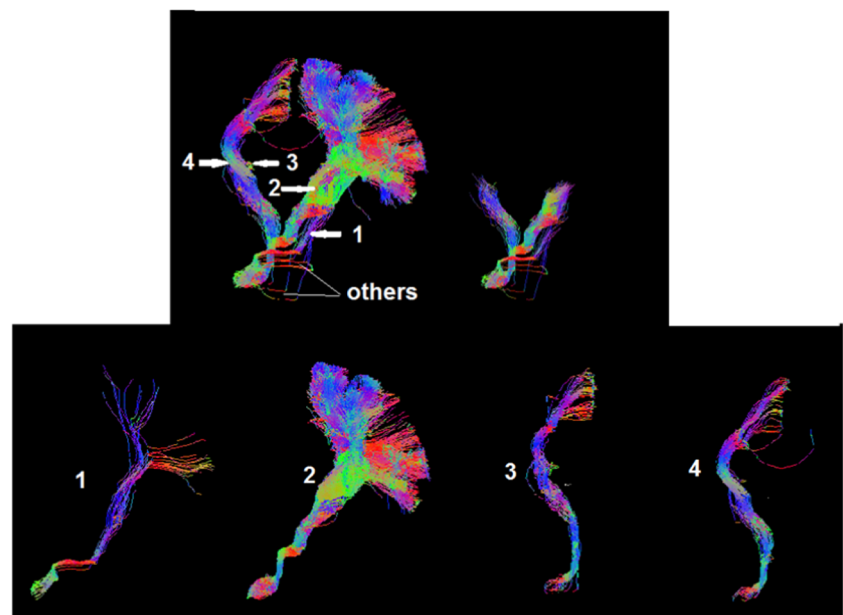
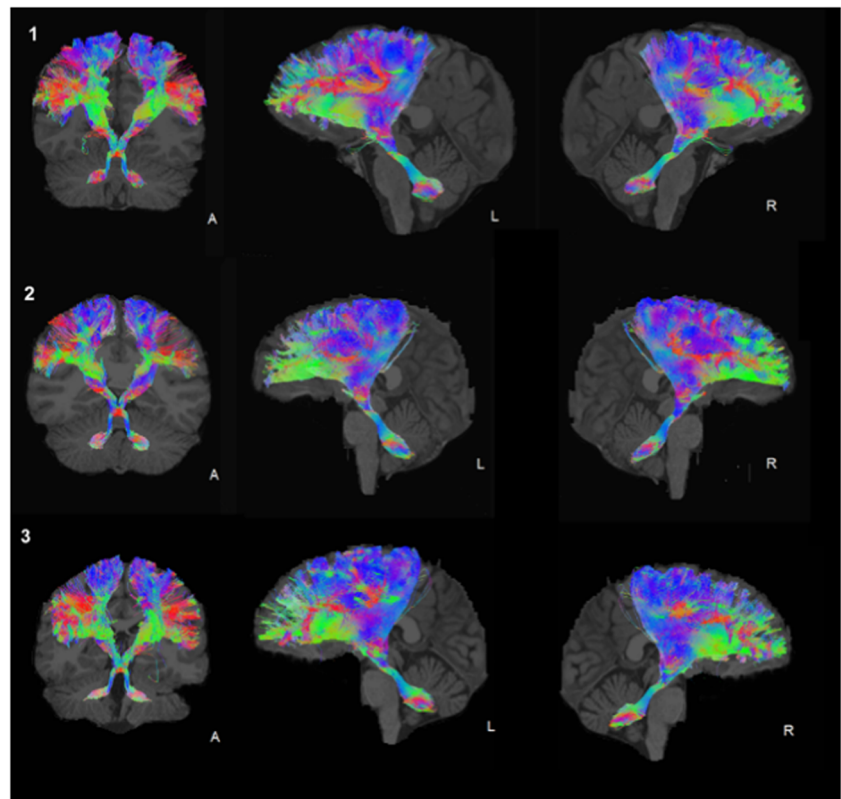


Fig. 5 The CTC trajectories for three subjects. For each row, the anterior, left lateral, and right lateral views of an individual CTC pathway are illustrated from left to right. The trajectories for the three individual CTC pathways are nearly identical for all of the subjects



Frontal Cortex Connections

As shown in Fig. 5, the fibers of the CTC pathway not only projected to the areas defined by ventral lateral and ventral anterior nuclei of the thalamus [16] but also extended to

prefrontal cortex. We used the Brodmann atlas to group fibers within the CTC pathway. The entire frontal cortex can be divided into 10 Brodmann areas (i.e., BA4, BA6, BA8–BA11, and BA44–BA47), as shown in Fig. 7a. We categorized each fiber in the CTC pathway by the Brodmann area in

Fig. 6 **a** The CTC pathway originated from the left and right dentate nuclei and **b** passed through the ipsilateral superior cerebellar peduncles (SCP). **c** Both the left and right CTC pathways decussated at the same place (DEC), just above the pontomesencephalic junction, and **d** passed through the contralateral red nuclei, **e** contralateral thalamus, and **f** the left and right internal capsules before reaching the frontal cortex

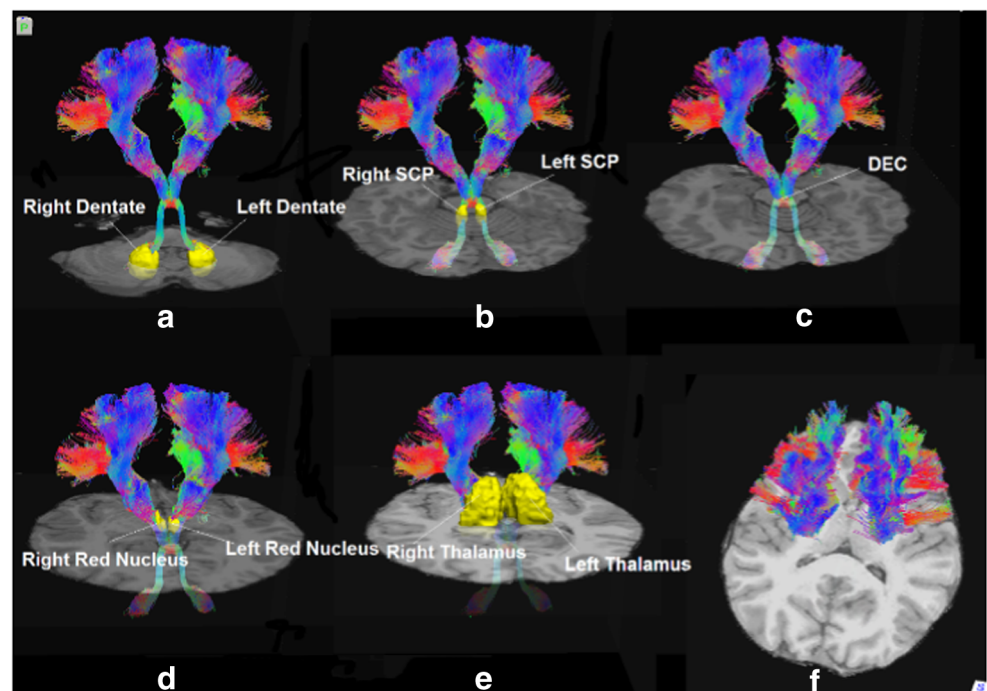
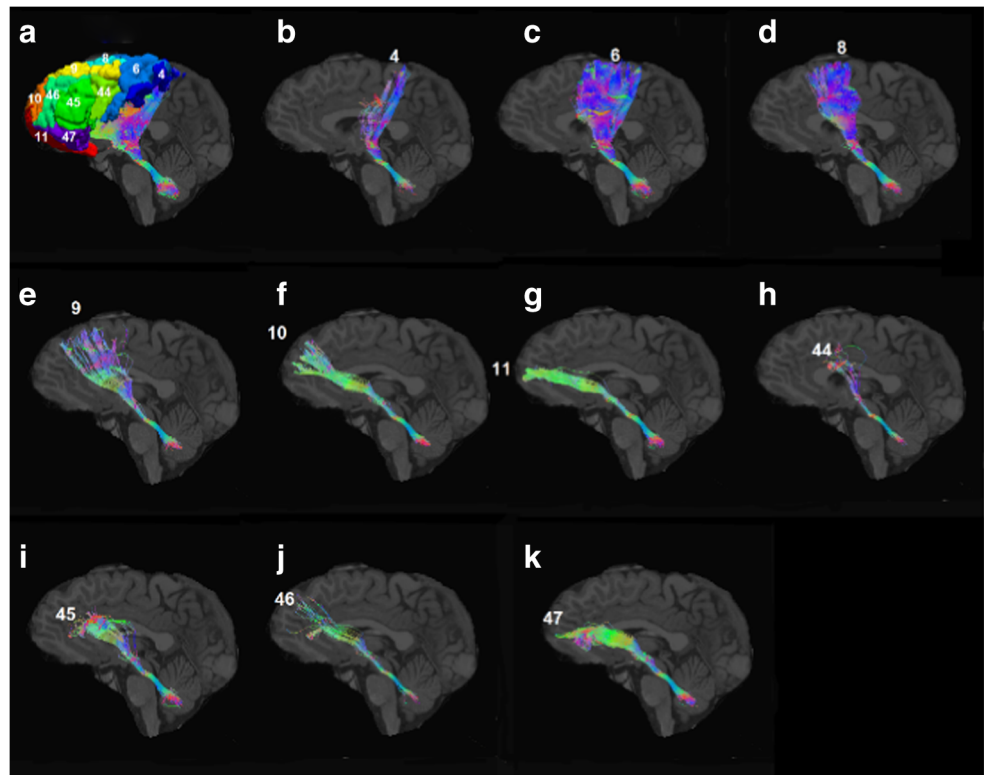


Fig. 7 CTC fibers categorized according to the areas of the Brodmann atlas. **a** Brodmann areas corresponding to the frontal cortex (BA4, BA6, BA8–BA11, and BA44–BA47). Fibers assigned to **b** BA4, **c** BA6, **d–f** BA8–BA11, and **g–k** BA44–BA47



which it terminated. Figure 7b–k illustrates the trajectories of those 10 fiber bundles. We also quantified the distribution of fibers that terminated in each Brodmann area and normalized those counts by the total number of fibers in the CTC pathway as shown in Fig. 8 for all subjects. Among all 10 Brodmann areas in the frontal cortex, the dominant area in which the CTC fibers terminated was BA6 (approximately 30–80% of fibers). Many previous studies have identified the link between motor and nonmotor functions with cerebellar output.

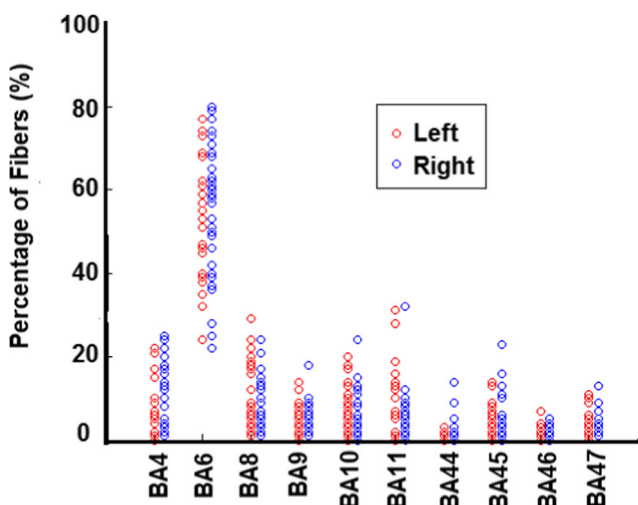


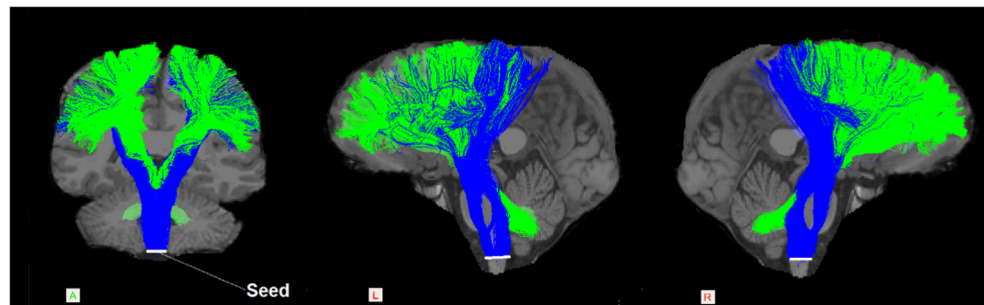
Fig. 8 CTC fiber distributions over 10 Brodmann areas. The percentage of fibers (fibers terminated in each area were normalized by the total number of fibers in a CTC tract) for each Brodmann area for all subjects. BA6 was the dominant area

We grouped the frontal cortex into motor and nonmotor areas such that BA4 and BA6 formed the motor areas (BA4 was primary and BA6 was premotor), and the rest of the prefrontal cortex (BA8–BA11 and BA44–BA47) formed the nonmotor area. We found that the distribution of CTC streamlines that terminated in motor and nonmotor areas were in a ratio of 7 to 3, respectively (Fig. 8). It was noteworthy that the CTC pathway had direct connection with BA44 and BA45 in the inferior frontal gyrus (Fig. 7h, i), which together form the Broca language area.

Spatial Relation With the Corticospinal Tract

The corticospinal tract is adjacent to the CTC pathway. To visualize the spatial relation between two adjacent tracts, we reconstructed the part of the corticospinal tract that connects the frontal cortex by using the same technique (i.e., seed volume inferior to brainstem and target of entire frontal cortex). Figure 9 demonstrates the spatial relation between the CTC pathway and corticospinal tract. From Fig. 9, we can see that the CTC joins the corticospinal tract at the midbrain. At the frontal cortex, the corticospinal tract predominantly terminated and overlapped with the CTC at the BA4 and BA6 areas, and very few tracts terminated at the prefrontal cortex.

Fig. 9 Spatial relationship between the CTC and corticospinal tract. **a–c** Anterior, left lateral, and right lateral views of the CTC (green) and corticospinal tract (blue). The white area below the brain stem served as the seed volume to reconstruct the corticospinal tract



Tract Length and Microstructures

Each streamline in the CTC bundle traverses the brain and has a spatial length. The mean length can be obtained by averaging the lengths of all streamlines in the bundle. We used existing, precalculated, fractional anisotropy (FA) and mean diffusivity (MD) maps combined with the streamlines of the left CTC (i.e., connection from the left DN to the right frontal lobe) and the right CTC (i.e., connection from the right DN to the left frontal lobe) pathways to calculate the mean FA and MD values for each pathway. The mean length was 134.3 ± 3.6 mm for the left CTC and 136.0 ± 3.5 mm for the right CTC pathway across all subjects. The mean FA and MD were 0.477 ± 0.025 and 0.728 ± 0.028 ($10^{-6} \text{ mm}^2 \text{ s}^{-1}$), respectively, for the left CTC and 0.491 ± 0.026 and 0.687 ± 0.025 ($10^{-6} \text{ mm}^2 \text{ s}^{-1}$), respectively, for the right CTC pathway. The mean FA value of the right CTC pathway was slightly higher than that of the left, and the mean MD value of the right CTC was slightly lower than that of the left. We performed pair-wise comparison *t* tests of the FA and MD values between the left and right CTCs for all subjects. The FA value of the right CTC pathway was significantly higher than that of left pathway ($P < 0.001$), and the MD value of the right pathway was significantly lower than that of left pathway ($P < 0.001$). All but three of the subjects were right handed, and the images from all but one subject satisfied the pattern described above. In one left-handed subject, the pattern of FA and MD values for the left and right CTCs was opposite.

Discussion

We describe a relatively simple probabilistic fiber-tracking scheme to reconstruct the entire CTC pathway from the DN to the contralateral frontal cortex. Successful tracking relied on the choice of the multi-fiber model. In the fiber-tracing process, the long path and contralateral connection served as natural filters; therefore, no synaptic ROIs were required to constrain the tracking. We used a similarity-based fiber-clustering technique to separate the final pathway from noise fibers without losing any fibers. We successfully applied this method to reconstruct CTC pathways for 39 healthy subjects, thereby demonstrating the reliability and repeatability of the

approach. The DTI sequence used in this study was used in clinical evaluations and was not optimized for this study. Therefore, we can extend this method to analyze data obtained from patients, such as patients presenting with clinical signs and symptoms indicative of injury to the proximal efferent cerebellar pathway after surgery for posterior fossa tumors (e.g., postoperative cerebellar mutism syndrome). We used DTI tractography to demonstrate that the DN in cerebellum is not only predominantly connected with cortical motor areas (BA4 and BA6) but also directly connected with many important prefrontal areas, such as the dorsal lateral prefrontal area (BA9 and BA46) and the Broca language area (BA44 and BA45). The prefrontal areas play an important role in working memory, cognition flexibility, planning, and abstract thinking [33, 34], whereas the Broca area is directly linked to language comprehension and speech production [35]. The CTC pathway at the level of the cerebellum is an integral fiber bundle. If it is damaged, functions supported by the entire contralateral prefrontal cortex are affected. Our technique can be easily developed further to include quantitation of injury to the proximal efferent cerebellar pathway and used to longitudinally monitor recovery. This is a clinically relevant application for patients with postoperative cerebellar mutism syndrome.

Conclusion

We proposed and tested a novel and robust method to define the CTC pathway in the human brain. We clearly demonstrated that a multi-fiber probabilistic model is required for CTC pathway reconstruction. By using the proposed method, the entire white matter fiber tracts spanning from the DN to the contralateral frontal cortex can be obtained. This pathway connects many important synaptic structures, such as SCPs, RNs, the thalamus, and the entire contralateral frontal cortex. We have shown that the DN not only predominantly connects with the primary and premotor cortex but also directly connects with many important prefrontal areas, which include the dorsolateral prefrontal and Broca language areas. Our findings provide direct structural evidence that the DN in the cerebellum plays an important role in many higher executive functions of the brain beyond coordination of movement.

Compliance with Ethical Standards

Conflict of Interest The authors declare that they have no conflict of interest.

References

- Patay Z, Enterkin J, Harreld JH, Yuan Y, Lobel U, Rumboldt Z, et al. MR imaging evaluation of inferior olivary nuclei: comparison of postoperative subjects with and without posterior fossa syndrome. *AJNR Am J Neuroradiol*. 2014;35(4):797–802.
- Middleton FA, Strick PL. Cerebellar output: motor and cognitive channels. *Trends Cogn Sci*. 1998;2(9):348–54.
- Schmahmann JD. The cerebellum and cognition. *Neurosci Lett*. 2019;688:62–75.
- van Baarsen K, Kleinnijenhuis M, Konert T, Cappellen v, van Walsum AM, Grotenhuis A. Tractography demonstrates dentate-rubro-thalamic tract disruption in an adult with cerebellar mutism. *Cerebellum*. 2013;12(5):617–22.
- Oh ME, Driever PH, Khajuria RK, Rueckriegel SM, Koustenis E, Bruhn H, et al. DTI fiber tractography of cerebro-cerebellar pathways and clinical evaluation of ataxia in childhood posterior fossa tumor survivors. *J Neuro-Oncol*. 2017;131(2):267–76.
- Avula S, Mallucci C, Kumar R, Pizer B. Posterior fossa syndrome following brain tumour resection: review of pathophysiology and a new hypothesis on its pathogenesis. *Childs Nerv Syst*. 2015;31(10):1859–67.
- Gudrunadottir T, Morgan AT, Lux AL, Walker DA, Walsh KS, Wells EM, et al. Consensus paper on post-operative pediatric cerebellar mutism syndrome: the Iceland Delphi results. *Childs Nerv Syst*. 2016;32(7):1195–203.
- Miller NG, Reddick WE, Kocak M, Glass JO, Lobel U, Morris B, et al. Cerebellocerebral diaschisis is the likely mechanism of post-surgical posterior fossa syndrome in pediatric patients with midline cerebellar tumors. *AJNR Am J Neuroradiol*. 2010;31(2):288–94.
- Schuepbach WM, Rau J, Knudsen K, Volkmann J, Krack P, Timmermann L, et al. Neurostimulation for Parkinson's disease with early motor complications. *N Engl J Med*. 2013;368(7):610–22.
- Flora ED, Perera CL, Cameron AL, Maddern GJ. Deep brain stimulation for essential tremor: a systematic review. *Mov Disord*. 2010;25(11):1550–9.
- Schlaier JR, Beer AL, Faltermeier R, Fellner C, Steib K, Lange M, et al. Probabilistic vs. deterministic fiber tracking and the influence of different seed regions to delineate cerebellar-thalamic fibers in deep brain stimulation. *Eur J Neurosci*. 2017;45(12):1623–33.
- Lehericy S, Grand S, Pollak P, Poupon F, Le Bas JF, Limousin P, et al. Clinical characteristics and topography of lesions in movement disorders due to thalamic lesions. *Neurology*. 2001;57(6):1055–66.
- Marx JJ, Iannetti GD, Thomke F, Fitzek S, Galeotti F, Truini A, et al. Topodiagnostic implications of hemiataxia: an MRI-based brainstem mapping analysis. *Neuroimage*. 2008;39(4):1625–32.
- Mori S, Crain BJ, Chacko VP, van Zijl PC. Three-dimensional tracking of axonal projections in the brain by magnetic resonance imaging. *Ann Neurol*. 1999;45(2):265–9.
- Kwon HG, Hong JH, Hong CP, Lee DH, Ahn SH, Jang SH. Dentatorubrothalamic tract in human brain: diffusion tensor tractography study. *Neuroradiology*. 2011;53(10):787–91.
- Behrens TE, Johansen-Berg H, Woolrich MW, Smith SM, Wheeler-Kingshott CA, Boulby PA, et al. Non-invasive mapping of connections between human thalamus and cortex using diffusion imaging. *Nat Neurosci*. 2003;6(7):750–7.
- Sun C, Wang Y, Cui R, Wu C, Li X, Bao Y, et al. Human thalamic-prefrontal peduncle connectivity revealed by diffusion spectrum imaging fiber tracking. *Front Neuroanat*. 2018;12:24.
- Law N, Greenberg M, Bouffet E, Laughlin S, Taylor MD, Malkin D, et al. Visualization and segmentation of reciprocal cerebrocerebellar pathways in the healthy and injured brain. *Hum Brain Mapp*. 2015;36(7):2615–28.
- Palesi F, Tournier JD, Calamante F, Muhlert N, Castellazzi G, Chard D, et al. Contralateral cerebello-thalamo-cortical pathways with prominent involvement of associative areas in humans in vivo. *Brain Struct Funct*. 2015;220(6):3369–84.
- Kamali A, Kramer LA, Frye RE, Butler IJ, Hasan KM. Diffusion tensor tractography of the human brain cortico-ponto-cerebellar pathways: a quantitative preliminary study. *J Magn Reson Imaging*. 2010;32(4):809–17.
- Karavasilis E, Christidi F, Velonakis G, Giavri Z, Kelekis NL, Efsthathopoulos EP, et al. Ipsilateral and contralateral cerebro-cerebellar white matter connections: a diffusion tensor imaging study in healthy adults. *J Neuroradiol*. 2018.
- Tournier JD, Calamante F, Connelly A. Robust determination of the fibre orientation distribution in diffusion MRI: non-negativity constrained super-resolved spherical deconvolution. *Neuroimage*. 2007;35(4):1459–72.
- Jeong JW, Chugani DC, Behen ME, Tiwari VN, Chugani HT. Altered white matter structure of the dentatorubrothalamic pathway in children with autistic spectrum disorders. *Cerebellum*. 2012;11(4):957–71.
- Granziera C, Schmahmann JD, Hadjikhani N, Meyer H, Meuli R, Wedeen V, et al. Diffusion spectrum imaging shows the structural basis of functional cerebellar circuits in the human cerebellum in vivo. *PLoS One*. 2009;4(4):e5101.
- Oldfield RC. The assessment and analysis of handedness: the Edinburgh inventory. *Neuropsychologia*. 1971;9(1):97–113.
- Fischl B, van der Kouwe A, Destrieux C, Halgren E, Segonne F, Salat DH, et al. Automatically parcellating the human cerebral cortex. *Cereb Cortex*. 2004;14(1):11–22.
- Desikan RS, Segonne F, Fischl B, Quinn BT, Dickerson BC, Blacker D, et al. An automated labeling system for subdividing the human cerebral cortex on MRI scans into gyral based regions of interest. *Neuroimage*. 2006;31(3):968–80.
- Behrens TE, Berg HJ, Jbabdi S, Rushworth MF, Woolrich MW. Probabilistic diffusion tractography with multiple fibre orientations: what can we gain? *Neuroimage*. 2007;34(1):144–55.
- Diedrichsen J. A spatially unbiased atlas template of the human cerebellum. *Neuroimage*. 2006;33(1):127–38.
- Besachio D, Quigley E, 3rd, Orlandi R, Harnsberger H and Wiggins R, 3rd. Myxoma of the vomer bone. *J Radiol Case Rep* 2013; 7(1): 12–17.
- Harnsberger HR. Diagnostic imaging. Head and neck. Salt Lake City: Amirsys; 2011.
- Ding Z, Gore JC, Anderson AW. Classification and quantification of neuronal fiber pathways using diffusion tensor MRI. *Magn Reson Med*. 2003;49(4):716–21.
- Elliott R. Executive functions and their disorders. *Br Med Bull*. 2003;65:49–59.
- Chan RC, Shum D, Touloupoulou T, Chen EY. Assessment of executive functions: review of instruments and identification of critical issues. *Arch Clin Neuropsychol*. 2008;23(2):201–16.
- Dronkers NF, Plaisant O, Iba-Zizen MT, Cabanis EA. Paul Broca's historic cases: high resolution MR imaging of the brains of Leborgne and Lelong. *Brain*. 2007;130(Pt 5):1432–41.

Publisher's Note Springer Nature remains neutral with regard to jurisdictional claims in published maps and institutional affiliations.